

Available online at www.sciencedirect.com

ScienceDirect

journal homepage: www.elsevier.com/locate/he



Active disturbance rejection control of metal hydride hydrogen storage



Alicia Li Jen Keow, Amy Mayhall, Marzia Cescon, Zheng Chen*

Department of Mechanical Engineering, University of Houston, Houston, TX 77204, USA

HIGHLIGHTS

- Modeling of metal hydride.
- Active disturbance rejection control (ADRC) of metal hydride.
- Estimation of the state-of-charge (SOC).
- Validation of the ADRC and SOC estimation.

ARTICLE INFO

Article history: Received 2 July 2020 Received in revised form 20 August 2020 Accepted 21 September 2020 Available online 11 October 2020

Keywords: Hydrogen storage Metal hydride Active disturbance rejection control

ABSTRACT

Metal hydride (MH) hydrogen storage is used in both mobile and stationary applications. MH tanks can connect directly to high-pressure electrolyzers for on-demand charging, saving compression costs. To prevent high hydrogen pressure during charging, hydrogen generation needs to be controlled with consideration for unknown disturbances and timevarying dynamics. This work presents a robust control system to determine the appropriate mass flow rate of hydrogen, which the water electrolyzer should produce, to maintain the gaseous hydrogen pressure in the tank for the hydriding reaction. A controloriented model is developed for MH hydrogen storage for control system design purposes. A proportional-integral (PI) and an active disturbance rejection control (ADRC) feedback controllers are investigated, and their performance is compared. Simulation results show that both the PI and ADRC controllers can reject both noises from the output measurements and unknown disturbances associated with the heat exchanger. ADRC excels in eliminating disturbances produced by the input mass flow rate, maintaining the pressure of the tank at the charging pressure with little oscillations. Additionally, the parameters estimated by the ADRC's extended state observer was used to predict the state-of-charge (SOC) of the MH.

© 2020 Hydrogen Energy Publications LLC. Published by Elsevier Ltd. All rights reserved.

Introduction

A hydrogen-powered fuel cell produces electricity with zero greenhouse gas. The fuel can be supplied by hydrogen stored in metal hydride (MH) tanks [1-5]. Hydrogen stored in MH

tanks is high in purity, which meets the fuel cells' requirements and avoids poisoning the stack [6]. Additionally, MH hydrogen storage operates under mild conditions, has few moving parts, and is safe and reliable [7]. MH hydrogen storage generally has a high energy density by volume but low energy

^{*} Corresponding author. W208 Engineering Building II, 4726 Calhoun Rd., Houston, TX, 77204, USA.
E-mail addresses: akeow@uh.edu (A.L.J. Keow), amayhall@uh.edu (A. Mayhall), mcescon2@uh.edu (M. Cescon), zchen43@central.uh.edu (Z. Chen).

density by weight. Each MH tanks' storage capacity, pressure, and reaction rate are customizable by proper selection of alloy used [4]. MH hydrogen storage has found its applications as a stationary energy storage system or in vehicles such as forklifts, where added mass for stability is desired [8,9].

Conventionally, MH tanks are charged at constant pressure by a high-pressure hydrogen tank [10]. A regulator is used to maintain constant pressure by controlling the flow of hydrogen. However, some facilities may not permit the storage of pressurized hydrogen tanks. In such circumstances, hydrogen is provided on-demand using water electrolysis. These hydrogen produced are compressed before storage in the MH tank. However, compression cost is high and remains the major contributor to the capital costs for hydrogen refueling stations [11]. Nevertheless, recently developed polymer electrolyte membrane (PEM) electrolyzers can produce hydrogen up to 30-45 MPa Pa [12]. This allows for direct storage of the produced hydrogen in the MH tank and eliminates the need for compressors and pumps. Combining electrolyzer and fuel cell with MH hydrogen storage provides flexibility for choosing appropriate power output, recharge rate, and energy storage to meet application demand [13].

Feasibility study, efficiency, and system configuration related to the charging of MH tanks using water electrolysis have been investigated. Laurencelle et al. designed the system for charging MH with electrolyzer [14]. Their work focused on MH material selection and sizing based on electrolyzer's specification and performed efficiency analysis. Varkaraki et al. charged the MH with a water electrolyzer using a fixed hydrogen flow rate until the system reaches a certain pressure [15]. This charging method cannot ensure that the tank is fully charged as it does not monitor the state-of-charge (SOC). Zhu et al. developed a method to estimate the SOC of MH hydrogen storage under static conditions. Still, this model is not applicable during the dynamic charging and discharging process [16]. Pérez-Herranz et al. designed a proportional-integral (PI) controller to regulate the hydrogen pressure in a temporary storage vessel of the alkaline electrolyzer system before a pump compresses the hydrogen for storage in MH tank [17]. Their work focuses on investigating the electrical and thermal properties of the electrolyzer under pressurized conditions. Raju et al. investigated the coupling of wind turbines with electrolyzers to charge MH [18]. Their work focuses on the heat exchanger operation to cool down the tank during charging with unpredictable hydrogen flow generated by turbulent wind velocity. Ogumerem et al. used model predictive control (MPC) to create pressure set-points to charge the MH so that the temperature of the tank is controllable by a heat exchanger [19]. They assumed compressed hydrogen in a high-pressure tank could supply hydrogen at any desired pressure during charging. Bhogilla et al. investigated short duration energy utilization of MH storage system using intermittent wind and solar energy for water electrolysis [20,21], while Endo et al. explored longer duration, up to 48 h, energy utilization for a similar system [22,23]. Bhogilla et al. and Endo et al. are only concern with the power transfer, efficiency and losses between each component and does not investigate the charging and discharging of MH tank [20-23].

There is a lack of literature addressing the issue associated with directly charging a MH tank with water electrolysis. One

difficulty with charging the tank is the indirect measurement of the absorption rate and SOC. Ideally, the hydrogen production rate should match the absorption rate to maintain the tank's pressure. Nevertheless, the absorption rate is influenced by temperature, pressure, and SOC. Exothermic absorption reaction causes these parameters to vary. If the tank were charged with a constant hydrogen flow rate until the tank reaches the desired pressure, the increase in the tank's temperature due to the exothermic reaction would produce false pressure and SOC reading. In a practical situation, disturbances exist during the charging operation. These disturbances could arise from unknown heat exchanger inputs such as coolant temperature and flow rate, leakage of the hydrogen from the inlet, and noise from the sensor measurement. A proper controller should be able to regulate the pressure despite the presence of such disturbances. A robust feedback controller should predict the reaction rate and produce a control signal for generating hydrogen to maintain pressure.

In this work, an active disturbance rejection control (ADRC) is developed to generate control signals for operating an electrolyzer, which produces hydrogen to maintain the MH tank's pressure during charging amid load disturbance and measurement noise. To enable ADRC control design, a control-oriented model is developed for MH hydrogen storage. The model captures the dynamics of the charging process and is presented in state space. The ADRC consists of three parts: the transient profile generator, the extended state observer, and the nonlinear controller. The transient profile generator produces a smooth reference pressure to drive the tank's pressure from the existing set-point to the new set-point. Proper reference selection prevents the sudden spike in the absorption reaction and avoids elevating the tank temperature past the safe operating limit. The extended state observer estimates the unknown system parameters, such as disturbances and absorption reaction rate. The nonlinear controller uses the estimates from the extended state observer to produce a suitable control signal to track the pressure reference while rejecting impacts of disturbances. The ADRC can also predict the SOC in real-time using the by-product of the extended state observer, making the ADRC more valuable in the hydrogen storage industry. The ADRC's performance is then compared against the well-known PI controller. The ADRC's ability to reject disturbances is highlighted. Both controllers were evaluated on a nonlinear model that described the MH hydriding and dehydriding reaction derived using mass and energy conservation. A heat exchanger model is included with the MH model to maintain the system's temperature within the safe operating limit.

The paper is organized as follows: section MH system model provides the MH tank with the heat exchanger model, and section controller design discusses controller design methodology. In section results and discussion, the simulation results are presented and discussed. Finally, the conclusions are provided in section Conclusion.

MH system model

The model representing the absorption and desorption of hydrogen in a MH tank coupled with heat exchanger was developed by Ref. [24,25] and is summarized here for completeness. Zhu et al. later developed a particle swarm optimization (PSO) algorithm to identify parameters in the model for MH container filled unknown metal alloy [26]. The model incorporates the mass and energy balance applied to the gaseous hydrogen and MH in the tank. Fig. 1 depicts the schematic of the MH system. ρ_g and ρ_s are the density of gaseous hydrogen and metal hydride, respectively. P and T are the tank pressure and temperature, respectively. fin is the mass flow rate of hydrogen into the tank. f_r is the absorption/ desorption rate. Q is the heat transfer with the circulating coolant. $T_{\rm w,\;in}$ and $T_{\rm w,\;out}$ are the temperature of the coolant in and out of the heat exchanger, respectively. fw is the mass flow rate of the coolant. $-\Delta H$ is the negative change in enthalpy for absorption. For this system, the tank has one inlet. Hydrogen in the tank can exist in two different forms; in gaseous form or reacts with metal alloys reversibly forming hydride. A heat exchanger system cools or heats the tank to aid the hydriding and dehydriding reaction.

The following assumptions were made when devising the model of the MH system with a heat exchanger:

- 1. Hydrogen gas is ideal.
- 2. Physical characteristics of the MH, such as thermal conductivity, porosity, and volume, remain constant throughout the hydriding and dehydriding reaction.
- 3. The whole tank and MH have the same temperature.
- 4. Heat convection inside the tank, temperature dependence of thermo-physical values, and radiative transfer in a porous medium is ignored.
- 5. Heat transfer coefficients are assumed constant.

The chemical equation representing the hydriding dehydriding reaction is

$$M(s) + \frac{x}{2}H_2(g) \underset{desorption}{\overset{absorption}{\rightleftharpoons}} MHx(s) + heat.$$
 (1)

where M is a metal alloy, and (s) and (g) refer to the solid and gas states, respectively. The hydriding reaction is exothermic while dehydriding reaction is endothermic. The x number of hydrogen atom H absorbed per mole of metal atom M depends on the type of metal alloy.

Let $f_{\rm in} = \bar{f}_{\rm in}/V_{\rm MH}$ represent the mass flow rate of hydrogen into the tank, normalized with V_{MH}. As hydrogen produced by

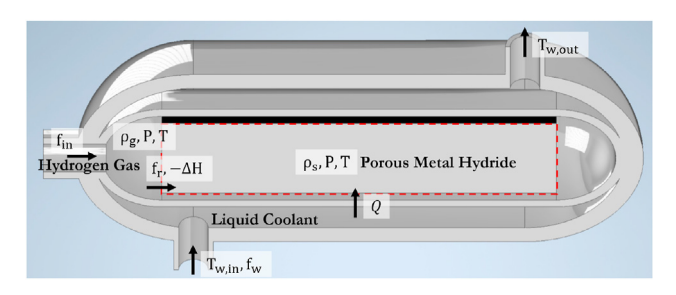


Fig. 1 - Schematic of a metal hydride tank. Adaptation of 24].

the water electrolyzer enters the tank, the density of gaseous hydrogen in the tank ρ_g increases. This is represented by $\dot{\rho}_g = \frac{J_{im} - J_r}{V_1},$

$$\dot{\rho}_{g} = \frac{f_{\text{in}} - f_{r}}{V_{1}},\tag{2}$$

where f_r is the rate of absorption/desorption of hydrogen and V₁ is the normalized volume representing the empty space not filled with powdered metal alloy. The volume of the void space in the tank where the gaseous hydrogen can occupy is,

$$V_1 = \frac{V_{\text{tank}}}{V_{\text{MH}}} - 1 + \varepsilon, \tag{3}$$

where V_{tank} is the volume of the tank, V_{MH} is the volume of the metal alloy, and ε is the porosity of the metal alloy. The current I used for electrolysis is proportional to the mass flow rate of hydrogen, represented by

$$\bar{f}_{\rm in} = \frac{I}{2F} N_{\rm cell} M_{\rm H_2}, \tag{4}$$

where F is the Faraday's constant, N_{cell} is the number of electrolyzer stack, and M_{H_2} is the molar mass of hydrogen.

The absorption and desorption kinetics of the metal alloy f_r is represented by [27]

$$f_{r} = \begin{cases} C_{a}e^{-\frac{E_{a}}{RT}}ln\left(\frac{P}{P_{eq, a}}\right)(\rho_{ss} - \rho_{s}) & , P > P_{eq, a}, \\ C_{d}e^{-\frac{E_{d}}{RT}}\left(\frac{P - P_{eq, d}}{P_{eq, d}}\right)(\rho_{s} - \rho_{s0}) & , P < P_{eq, d}, \end{cases}$$

$$0 & , otherwise.$$
(5)

where P and T are the pressure and temperature of the MH tank, respectively, R is the gas constant, ρ_s is the density of the MH, Ca and Cd are the absorption and desorption constants, respectively, Ea and Ed are the activation energy for absorption and desorption, respectively, $P_{eq, a}$ and $P_{eq, d}$ are the equilibrium pressure for absorption and desorption, respectively, ρ_{ss} is the density of the saturated metal alloy after it has fully absorbed all gaseous hydrogen that it can reversibly desorb and ρ_{s0} is the density of the metal alloy after it has desorbed all hydrogen.

When the pressure of the gaseous hydrogen in the tank is larger than the equilibrium pressure for absorption, then hydrogen will react with the metal alloy to form MH. Similarly, if the pressure of the gaseous hydrogen in the tank is lower than the equilibrium pressure for desorption, then the hydrogen gas are separated from the metal alloy. The equilibrium pressure is provided by the pressure composition and temperature (PCT) curve, which represents the thermodynamic aspects of the hydride formation. The curves are approximated using [28]

$$P_{eq} = P_0 \cdot e^{\left(a - \frac{b}{T} + (\phi \pm \phi_0) \tan \left(\pi \left(\frac{H}{H_{max}} - 0.5\right)\right) \pm \frac{\beta}{2}\right)}, \tag{6}$$

where $P_{\rm eq}$ is the equilibrium pressure, P_0 is the atmospheric pressure, a and b are fitting coefficient, φ and φ_0 represents the plateau flatness, β represents the hysteresis factor, + is for absorption and - is for desorption. The state-of-charge (SOC) of the MH is represented by

$$\frac{H}{H_{\text{max}}} = \frac{\rho_{\text{s}} - \rho_{\text{s0}}}{\rho_{\text{sc}} - \rho_{\text{s0}}}.\tag{7}$$

The hydrogen gas in the tank obey the state equation

$$P = \rho_{\rm g} T \frac{R}{M_{\rm Ho}}.$$
 (8)

The density of the MH $\rho_{\rm s}$ changes with the absorption and desorption reaction and is represented by

$$\dot{\rho}_{\rm s} = \frac{f_{\rm r}}{V_2},\tag{9}$$

where $V_2 = 1 - \varepsilon$ is the normalized volume of the MH.

The absorption process is exothermic while the desorption process is endothermic. The energy balance is described by

$$V_1 C_{p, g} \frac{\partial (\rho_g T)}{\partial t} + V_2 C_{p, s} \frac{\partial (\rho_s T)}{\partial t} = \kappa_e \nabla^2 T + f_r \frac{\Delta H}{M_{H_2}} + \frac{Q}{V_{MH}}, \tag{10}$$

where $C_{\rm p,\ g}$ represents the specific heat of hydrogen gas, $C_{\rm p,\ s}$ is the specific heat of the metal alloy, $\kappa_{\rm e}$ is the thermal conductivity, ΔH is the heat of reaction, and Q is the amount of heat transfer from the circulating coolant to the MH tank. It is assumed that the temperature is uniformly distributed in the tank, thus the Laplacian of temperature in Eq. (10) is neglected. Using chain-rule, the following two equations are derived.

$$\frac{\partial \left(\rho_{g}T\right)}{\partial t} = T\left(\frac{f_{in} - f_{r}}{V_{1}}\right) + \rho_{g}\dot{T},\tag{11}$$

$$\frac{\partial(\rho_{s}T)}{\partial t} = T\left(\frac{f_{r}}{V_{2}}\right) + \rho_{s}\dot{T}.$$
(12)

The rate of change of the MH tank's temperature is determined by replacing Eqs. (11) and (12) in Eq. (10) and rearrange,

$$\dot{T} = \frac{-C_{p, g}(f_{in} - f_r)T - C_{p, s}f_rT + f_r\frac{\Delta H}{M_{H_2}} + \frac{Q}{V_{MH}}}{V_1C_{p, g}\rho_g + V_2C_{p, s}\rho_s}.$$
(13)

The overall heat transfer between the MH tank and the circulating coolant is estimated by the heat balance model, and thus the outlet temperature of the circulating coolant $T_{\rm w,\,out}$ is represented by

$$dQ = U(T_w - T)dA = -f_w C_{p, w} dT_w, (14)$$

$$\int_{0}^{A_{s}} U(T_{w} - T) dA = - \int_{T_{w, in}}^{T_{w, out}} f_{w} C_{p, w} dT_{w},$$
(15)

$$T_{w,\,\mathrm{out}} = T + \left(T_{w,\,\mathrm{in}} - T\right) e^{\frac{UA_S}{\int_W C_{P,\,w}}}. \tag{16} \label{eq:two_sum}$$

where $f_{\rm w}$ is the mass flow rate of coolant, $C_{\rm p,~w}$ is the specific heat of coolant, $T_{\rm w,~in}$ is the temperature of coolant into the heat exchanger, U is the overall heat transfer coefficient, $A_{\rm s}$ is the area of contact between the circulating coolant and the MH tank. Q is expressed in terms of the inlet temperature of the coolant,

$$Q = -f_{w}C_{p, w}(T_{w, out} - T_{w, in}),$$
(17)

$$= f_{\mathbf{w}} C_{\mathbf{p}, \, \mathbf{w}} (T_{\mathbf{w}, \, \mathbf{in}} - T) \left(1 - e^{\frac{U_{\mathbf{A_s}}}{\int_{\mathbf{w}} C_{\mathbf{p}, \, \mathbf{w}}}} \right). \tag{18}$$

The mathematical model of the MH system is presented in state-space form for the design of advance control. Let the state vector, input vector, and output vector be

$$\mathbf{X} = \begin{bmatrix} x_1 \\ x_2 \\ x_3 \end{bmatrix} = \begin{bmatrix} \rho_{g} \\ \rho_{s} \\ T \end{bmatrix}, \ \mathbf{U} = \begin{bmatrix} u_1 \\ u_2 \\ u_3 \end{bmatrix} = \begin{bmatrix} f_{in} \\ f_{w} \\ T_{w,in} \end{bmatrix}, \tag{19}$$

$$\mathbf{Y} = \begin{bmatrix} \mathbf{y}_1 \\ \mathbf{y}_2 \end{bmatrix} = \begin{bmatrix} \mathbf{P} \\ T_{\text{w,out}} \end{bmatrix} \tag{20}$$

respectively. The system can be written in state-space form, $\dot{\mathbf{X}} = \mathcal{F}(\mathbf{X}, \mathbf{U})$ and $\dot{\mathbf{Y}} = \mathcal{G}(\mathbf{X}, \mathbf{U})$, as follows

$$\begin{bmatrix} \dot{x}_{1} \\ \dot{x}_{2} \\ \dot{x}_{3} \end{bmatrix} = \begin{bmatrix} \frac{u_{1} - f_{r}}{V_{1}} \\ \frac{f_{r}}{V_{2}} \\ -x_{3} \left(C_{p,g} u_{1} - f_{r} \left(C_{p,g} - C_{p,s} \right) \right) + f_{r} \frac{\Delta H}{M_{H_{2}}} + \frac{Q}{V_{MH}} \\ \frac{V_{1} C_{p,g} x_{1} + V_{2} C_{p,s} x_{2}}{V_{1} C_{p,s} x_{2}} \end{bmatrix}, (21)$$

$$\begin{bmatrix} y_1 \\ y_2 \end{bmatrix} = \begin{bmatrix} x_1 x_3 \frac{R}{M_{H_2}} \\ x_3 + (u_3 - x_3) e^{-\frac{UA}{u_2 \cdot p_1 \cdot w}} \end{bmatrix}, \tag{22}$$

where

$$Q = u_2 C_{p, w} (u_3 - x_3) \left(1 - e^{-\frac{UA}{u_2 C_{p, w}}} \right), \tag{23}$$

$$f_{r} = \begin{cases} C_{a}e^{-\frac{E_{a}}{Rx_{3}}}\ln\left(\frac{y_{1}}{P_{eq, a}}\right)(\rho_{ss} - x_{2}), \ y_{1} > P_{eq, a}, \\ C_{d}e^{-\frac{E_{d}}{Rx_{3}}}\left(\frac{y_{1} - P_{eq, d}}{P_{eq, d}}\right)(x_{2} - \rho_{s0}), \ y_{1} < P_{eq, d}, \end{cases}$$

$$0, \ otherwise,$$
(24)

$$P_{\text{eq, a}} = P_0 \cdot e^{\left(a - \frac{b}{x_3} + (\varphi + \varphi_0) \tan \left(\pi \left(\frac{x_2 - \rho_{s0}}{\rho_{ss} - \rho_{s0}} - 0.5\right)\right) + \frac{\beta}{2}\right)}, \tag{25}$$

$$P_{\text{ed. d}} = P_0 \cdot e^{\left(a - \frac{b}{x_3} + (\varphi - \varphi_0) \tan \left(\pi \left(\frac{x_2 - \rho_{80}}{\rho_{80} - \rho_{80}} - 0.5\right)\right) - \frac{\beta}{2}\right)}. \tag{26}$$

Controller design

Problem formulation

An empty MH tank can be charged using hydrogen produced from water electrolysis. Polymer electrolyte membrane (PEM) electrolyzers are operated in current mode, producing hydrogen at a rate proportional to current. The MH tank is charged by maintaining the gaseous pressure in the tank constant. The PCT curve gives this desired pressure based on the desired SOC. Exothermic absorption reaction will increase the tank's temperature while the heat exchanger decreases the temperature. The MH tank is fully charged to the desired SOC determined by the chosen charging pressure after the tank's temperature reaches equilibrium with the coolant temperature. A feedback controller must operate the electrolyzer to determine the input mass flow rate of hydrogen $(u_1=f_{\rm in})$ into the tank to maintain the output tank's pressure $(y_1=P)$ at the desired charging pressure.

A commonly used controller for set-point tracking is the proportional-integral (PI) controller [29]. The control signal u_1 produced by the PI controller is a linear combination of the tracking error between the measured output y_1 and desired output v, and the integral of this error. The control structure is as follows:

$$e(t) = v(t) - y_1(t), \tag{27}$$

$$u_1(t) = K_p e(t) + K_i \int e(t)dt, \tag{28}$$

where K_p and K_i are user-selected controller parameters. Large K_p will allow the system output y_1 to track v quickly. When K_p is too large, the output will overshoot the desired value. The integral term K_i reduces steady state error.

The PI controller is simple to implement and is insensitive to measurement noise. With proper tuning, the controller can make the system insensitive to load disturbances [30]. The most significant advantage of using a PI controller is that the controller can be tuned heuristically without knowing the model of the metal hydride system. Nevertheless, its advantage is also its weakness. Since the controller provides no information about the system, the SOC remains unknown.

This work aims to design a controller that maintains pressure during the charging of MH amid load disturbance and measurement noise and predicts the SOC of the MH tank. The active disturbance rejection control (ADRC) proposed by Ref. [31,32] is widely used to solve the motion control problem governed by Newton's law [33]. ADRC comprises of three main components: a) a tracking differentiator (TD), b) a nonlinear controller (NLC) and, c) an extended state observer (ESO).

In this work, the key concept from ADRC is applied to the MH system to simultaneously reject disturbances while charging the MH tank and predict SOC of the tank.

Transient profile generator

A step references v results in large error into the feedback controller causing the control signal to change abruptly. This large control signal corresponds to a high mass flow rate.

From Eq. (5), the absorption reaction is significant when the difference between P and P_{eq, a} is large. Similarly, the reaction is larger when the SOC is small. At low SOC, a sudden pressure increase leads to a spike in the absorption reaction, which could raise temperature past the safe operating limit $T_{\rm lim}$. Therefore, any step reference should be filtered to ensure that the error signal into the feedback controller changes continuously.

A smooth transient profile for the reference signal is generated using the following equation,

$$\dot{\mathbf{v}}_1 = \mathbf{v}_2, \tag{29}$$

$$\dot{v}_2 = -rf_{\text{sat}}(\vartheta, \delta),$$
 (30)

$$\vartheta = \upsilon_1 - \upsilon + \frac{\upsilon_2 |\upsilon_2|}{2r},\tag{31}$$

$$f_{\rm sat}(\vartheta, \delta) = \begin{cases} {\rm sgn}(\vartheta), & |\vartheta| > \delta, \\ & , \\ \frac{\vartheta}{\delta}, & |\vartheta| \leq \delta. \end{cases}$$
 (32)

where v is the desired set-point, v_1 is the generated transient profile, v_2 is the rate of change of v_1 and $f_{\rm sat}$ (A, δ) is a linear saturation function. The parameter r is a tuning parameter use to speed up or slow down the transient profile. The response speed of the system limits the transient profile generated by r.

Extended state observer

For ADRC design, the system's outputs are redefined as the tanks' temperature $y_1 = P$ and the tank's pressure $y_2 = T$, and the input is the hydrogen mass flow rate $u_1 = f_{\rm in}$. As hydrogen flows into the tank, the accumulation of hydrogen in the tank will increase the tank's pressure. At suitable pressure, the metal alloy will react with hydrogen. The formation of MH will reduce the pressure in the tank. Additionally, the heat emitted from the absorption process increases pressure, while heat transfer with circulating coolant decreases the pressure. It is difficult for the controller to determine the hydrogen mass flow into the tank $f_{\rm in}$ to maintain tank pressure P without an accurate knowledge of the absorption reaction rate.

Here, the complex relationship between ρ_g , T, \dot{T} and $\dot{\rho}_s$ are represented by the function f(t). This unknown function f(t) is estimated by the extended state χ_2 using input $u_1 = f_{\rm in}$ and output $y_1 = P$. Then, the knowledge are used by the controller to modify the control signal. The overall system is generalized as follow:

$$y_1 = \chi_1 = P, \tag{33}$$

$$\dot{\chi}_{1} = \rho_{g} \frac{R}{M_{H_{2}}} \dot{T} - \frac{TR}{M_{H_{2}}} \frac{V_{2}}{V_{1}} \dot{\rho}_{s} + \frac{TR}{M_{H_{2}}} \frac{1}{V_{1}} f_{in}, \tag{34} \label{eq:chi_1}$$

$$= f(t) + bu_1, \tag{35}$$

$$=\chi_2+bu_1,\tag{36}$$

$$\dot{\chi}_2 = \dot{f}(t). \tag{37}$$

It is assumed that $\frac{TR}{M_{H_2}}\frac{1}{V_1} \leq b$ is bounded. This assumption is valid if the system is always operating within the temperature limit, $T \leq T_{lim}$.

This system is always observable and the extended state observer has the following form,

$$\epsilon = \mathbf{z}_1 - \mathbf{\chi}_1, \tag{38}$$

$$\dot{z_1} = z_2 + bu_1 - \beta_{01} f_{e1}(\epsilon, \phi_{01}, \delta),$$
 (39)

$$\dot{z_2} = -\beta_{02} f_{e2}(\epsilon, \phi_{02}, \delta),$$
 (40)

where β_{01} and β_{02} are the observer gains. If the observer gains are selected appropriately, the states can be estimated such that $z_1 \approx \chi_1$ and $z_2 \approx \chi_2 = f(t)$. f_e (ϵ , ϕ , δ) is the modified exponential gain function for tracking the unknowns and has the form [31],

$$f_{e}(\epsilon, \phi, \delta) = \begin{cases} |\epsilon|^{\phi} \operatorname{sgn}(\epsilon), & |\epsilon| > \delta, \\ \frac{\epsilon}{\delta^{1-\phi}}, & |\epsilon| \leq \delta. \end{cases}$$
(41)

where $0 < \phi < 1$ is user selected. f_e (ϵ , ϕ , δ) will yield a high gain when the error is small. $\delta > 0$ is a small number used to limit the gain in the neighborhood of the origin.

With the unknown $\chi_2 = f(t)$ estimated, the controller can predict the pressure caused by both the absorption reaction and the heat transfer with circulating. Estimates z_1 and z_2 are used to modify the control signal.

Nonlinear feedback control

In Section Transient profile generator, the reference signal ν is modified to eliminate abrupt changing control signal while in Section Extended state observer, an observer is designed to estimate unknown system behavior. Here, a nonlinear feedback controller is designed to track the generated pressure reference ν_1 using the information predicted by the observer z_1 and z_2 . The feedback controller is represented by

$$e = v_1 - z_1, \tag{42}$$

$$u_0 = \kappa f_e(e, \psi, \delta),$$
 (43)

$$u_1 = \frac{u_0 - z_2}{h},$$
 (44)

where e is the error signal into the nonlinear controller, κ is the control gain, f_e (e, ψ , δ) is the nonlinear function with ψ a user defined parameter Eq. (41), and u_1 is the input into the system with compensation for the estimated unknown.

Using the control law defined in Eq. (44), the system defined by Eq. (33) and Eq. (34) reduces to

$$y_1 = \chi_1, \tag{45}$$

$$\dot{\chi}_1 = u_0. \tag{46}$$

When the extended state observer accurately predict the disturbance χ_2 such that $z_2 \approx \chi_2 = f(t)$, the simplified system Eq. (46) is easily controlled. The overall controller schematic is illustrated by the block diagram in Fig. 2.

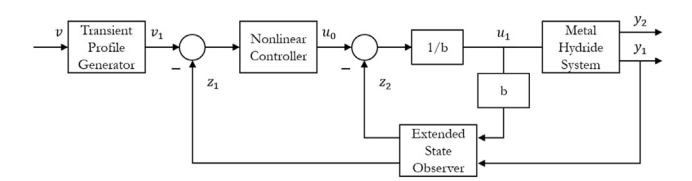


Fig. 2 – Block diagram representation of the MH system with active disturbance rejection control (ADRC), which comprise of the transient profile generator, nonlinear controller, and extended state observer.

State-of-charge estimator

During practical implementation of the system, the measurable values are the internal tank pressure $P_{\rm m}$, tank temperature $T_{\rm m}$, and input mass flow rate $f_{\rm in,\ m}$. The measurements obtained from the controller are $f_{\rm in}$ and z_2 . Therefore, rate of change of the solid density is estimated as

$$\dot{\rho}_{s,\;est} = -\frac{M_{H_2}}{T_m R} \frac{V_1}{V_2} \bigg(z_2 - \frac{P_m}{T_m} \dot{T}_m - \frac{T_m R}{M_{H_2}} \frac{1}{V_1} \bigg(f_{in,\;m} - f_{in} \bigg) \bigg), \tag{47} \label{eq:phis_spectrum}$$

where the rate of change of temperature measurement \dot{T}_m can be numerically calculated. The estimated solid density is

$$\rho_{s, \text{ est}} = \rho_{s, \text{ init}} + \int \dot{\rho}_{s, \text{ est}} dt, \tag{48}$$

where initial density of solid $\rho_{s, init}$ before absorption is found using the PCT curve with the initial temperature and pressure measurements at steady state. Therefore the SOC is estimated using

$$\left(\frac{H}{H_{\text{max}}}\right)_{\text{est}} = \frac{\rho_{\text{s, est}} - \rho_{\text{s0}}}{\rho_{\text{ss}} - \rho_{\text{s0}}}.$$
(49)

Results and discussion

System description

The MH hydrogen storage container used in this work is HBond-7000 L by LabTech Int. Ltd [34]. The technical specifications provided by the manufacturer are listed in Table 1.

The volume of the alloy is found using the mass $m_{\rm MH}$, density $\rho_{\rm SO}$ and porosity ε of the MH,

$$V_{\rm MH} = \frac{m_{\rm MH}}{\rho_{\rm en} \cdot \varepsilon}.$$
 (50)

Knowing the density of hydrogen $\rho_{\rm H_2}$ and the capacity of the alloy, the saturated alloy density $\rho_{\rm ss}$ is therefore,

Table 1 $-$ Technical Specifications of MH tank [34,35].		
Chemical Composition	(LaCe)Ni ₅	
Charging Pressure Charging Temperature Discharge Pressure	15 bar 20 – 25 °C 2 – 10 bar	
Discharge Temperature H ₂ Storage Capacity	10 - 30 °C 7000 L	
Alloy Mass	46 g	

Table 2 $-$ Parameters used in the metal hydride model [25,27,35,36].			
ε	0.5	ρ_{s0}	8400 kg/M ³
R	8.314 J/(mol K)	M_{H_2}	2 g/mol
m_{MH}	47 kg	V_{tank}	0.0165 m^3
V_{H_2}	7849 L	$ ho_{ m H_2}$	0.0897 kg/M ³
U	25 W/(m ² K)	A_s	1.347 m ²
C _{p, w}	1860 J (kg K)	$\rho_{\mathbf{w}}$	1000 kg/M ³
C _{p, s}	419 J/(kg K)	C _{p, g}	14,890 J/(kg K)
ΔH_a	30,478 J/mol	$\Delta H_{ m d}$	30,800 J/mol
C_a	59.187 1/s	C_d	9.57 1/s
Ea	21179.6 J/mol	E_d	16,420 J/mol
Po	101, 325 Pa	В	0.11414
Α	13.7	В	3704
Φ	0.33	φ ₀	0.008584

$$\rho_{ss} = \rho_{s0} \left(1 + \frac{V_{H_2}}{m_{MH}} \rho_{H_2} \right) \tag{51}$$

Parameters related to the MH tank, listed in Table 2, was identified and validated by Gonzatti et al. in Ref. [25,35,36].

On-off control simulation

The dynamic behavior of the MH system with a heat exchanger is simulated in MATLAB Simulink using

parameters in Table 2. The input to the heat exchanger remains unchanged with $f_w=0.1667~kg~s^{-1}$ and $T_{w,~in}=293.15~K$. The initial temperature of the tank is $T_i=293.15~K$ and the initial pressure is $P_i=101,~325~Pa$. The initial SOC estimated using $T_i,~P_i,~and~Eq$. (6) gives $\frac{H}{H_{max}i}=0.098$. From Eq. (7), the initial density of the solid is $\rho_{s,~i}=8412.4~kg/m^3$. From Eq. (8), the initial density of hydrogen gas is $\rho_{g,~i}=0.0831~kg/m^3$.

A simple on-off feedback controller is applied to charge the MH to 91%, which corresponds to a gas pressure of $P_{\rm ref}=1.5$ MPa at 293.15 K. The on-off controller is configured such that when the pressure of the tank is below $P_{\rm ref}$, the mass flow rate is constant at $f_{\rm in}=0.0012$ kg m⁻³ s⁻¹. When the pressure is above the charging pressure $P_{\rm ref}$, then the mass flow rate is zero, $f_{\rm in}=0$. The chosen $f_{\rm in}$ assumes the use of a 5 stack Giner ELX's HP PEMI high pressure electrolyzer, which is

rated up to 250 A per stack and can produce $f_{\rm in}=1.2955\times 10^{-5}$ kg s⁻¹ of hydrogen at 20 bar [37]. Normalize the production rate using $V_{\rm MH}$ gives $f_{\rm in}=0.0012$ kg m⁻³ s⁻¹.

The simulation results with on-off feedback control are presented in Fig. 3. The first graph compares the mass flow rate of hydrogen into the tank $f_{\rm in}$ against the absorption reaction $f_{\rm r}$. The second graph shows the pressure of gaseous hydrogen in the tank P, the equilibrium pressure for absorption $P_{\rm eq.}$ a, and the reference pressure $P_{\rm ref.}$ The third graph gives the tank's temperature T and the coolant temperature into $T_{\rm w,\ in}$ and out of the heat exchanger $T_{\rm w,\ out}$. The fourth

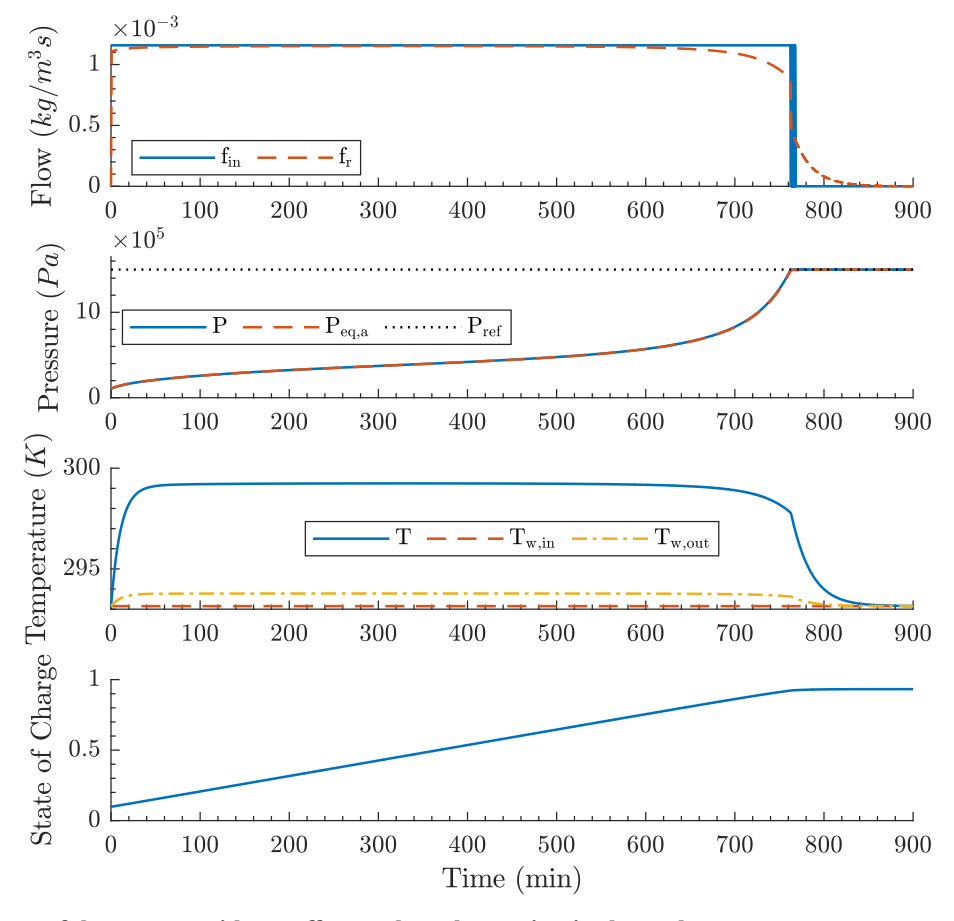


Fig. 3 – Performance of the system with on-off control used to maintain the tank pressure at $P_{ref} = 1.5$ MPa Pa during charging. When $P < P_{ref}$, $f_{in} = 0.0012$ kg m⁻³ s⁻¹, else, $f_{in} = 0$ kg m⁻³ s⁻¹.

graph shows the SOC of the tank. As shown in the first graph, before 762 min, the absorption rate is limited by $f_{\rm in}$. The temperature increases proportionally to the absorption reaction. As the SOC increases, the equilibrium pressure for absorption increases. Between 762–768 min, the controller switches the electrolyzer on and off rapidly to maintain pressure. When pressure difference between P and $P_{\rm eq,\ a}$ is large, the absorption rate is large. However, as SOC increases, the reaction rate decreases. With decreasing absorption, the heat generated decreases, and the heat exchanger can lower the tank temperature. After 768 min, as the temperature decreases, the pressure in the tank also decreases.

PI controller tuning

The proportional-integral (PI) controller is widely applied to solve set-point tracking issues in the process industry. Here, the PI controller is used to track the trajectory v_1 generated by Eq. (29) for $P_{\rm ref}=1.5$ MPa . The system parameters, initial conditions, and heat exchanger inputs are described in Section on-off control simulation.

The relay feedback tuning method is used to tune the PI controller gains [38,39]. In the tuning process, a heuristically chosen controller parameters first bring the system to a steady-state. At a steady-state, the PI controller is replaced by a biased relay. The biased relay has amplitude d and hysteresis width γ . The application of the biased relay causes the output y=P to oscillate. Hence, the error into the biased relay $e=v_1-P$ will also oscillate with amplitude A_u . The output of the biased relay is

$$u_{\text{relay}} = \begin{cases} +d, & A_{\text{u}} < -\gamma, \\ -d, & A_{\text{u}} > \gamma. \end{cases} \tag{52}$$

Using d and A_u, the ultimate gain K_u is found,

$$K_{\rm u} = \frac{4d}{\pi A_{\rm u}}.\tag{53}$$

The ultimate period $T_{\rm u}$ is the period of this oscillation. With the ultimate values identified, the traditional Ziegler-Nichols (ZN) tuning rule in Eq. (54) is applied to determine the PI controller gains which give the best disturbance rejection [40].

$$K_p = 0.45K_u, \quad K_i = 0.54\frac{K_u}{T_v}.$$
 (54)

The relay feedback tuning process is applied to the MH system in Fig. 4. During the tuning process, the PI controller first brings the system to a state P = 1 MPa Pa. Then, the biased relay with amplitude $d=\pm 0.1$ and hysteresis $\gamma=\pm 10$, 000 is applied to the system. Application of the relay result in a stable oscillation and the feedback signal $e=\nu-P$ has amplitude $A_u=10,\!040$ and period $T_u=0.3$, as shown in Fig. 5. The new PI controller parameters calculated using Eq. (54) are: $K_p=5.7068\times 10^{-6}$ and $K_i=2.2827\times 10^{-5}$.

Transient profile selection

Fig. 6 shows the comparison between two different pressure reference v_1 produced by the r value: r1=0.5 and r2=1 with $\delta=0.001$. The first graph shows the input $f_{\rm in}$ against reaction rate $f_{\rm r}$. The second graph shows the tank pressure P against transient profile v_1 . The third graph shows the tank temperature T against temperature limit $T_{\rm lim}$. The fourth graph presents the SOC and fifth shows the tracking error, $e=v_1-P$. As shown in Fig. 6, to maintain constant gas pressure during charging, the mass flow rate $f_{\rm in}$ should match the absorption reaction $f_{\rm r}$.

When r is large, the transient time is shorter and v_1 reaches the reference pressure v quickly. With shorter transient time,

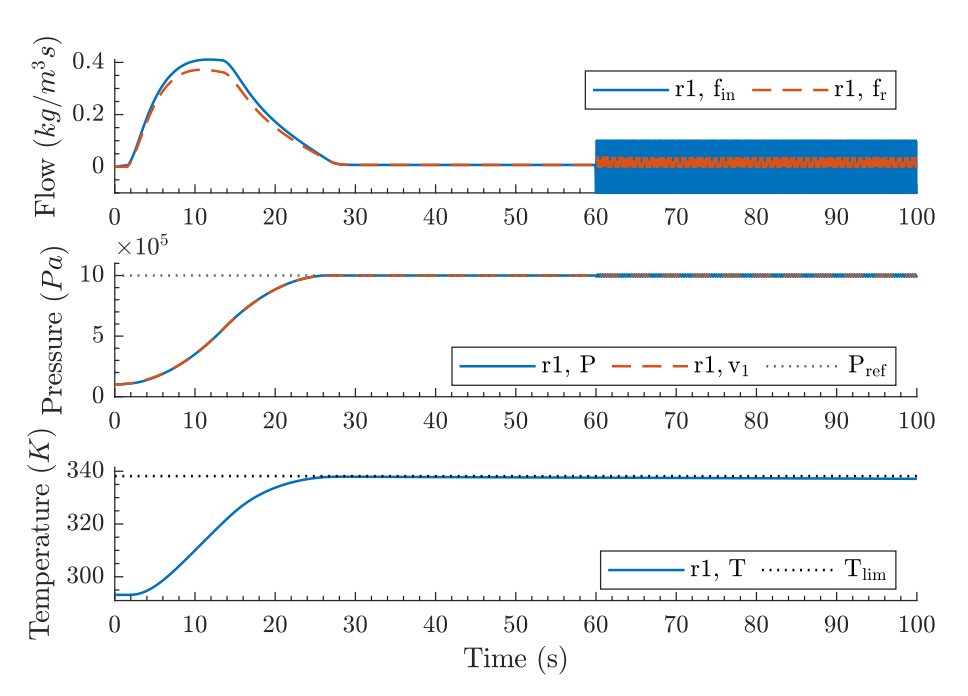


Fig. 4 – PI controller tuning using relay feedback method. The relay is activated after 60 s when the system reaches a steady-state.

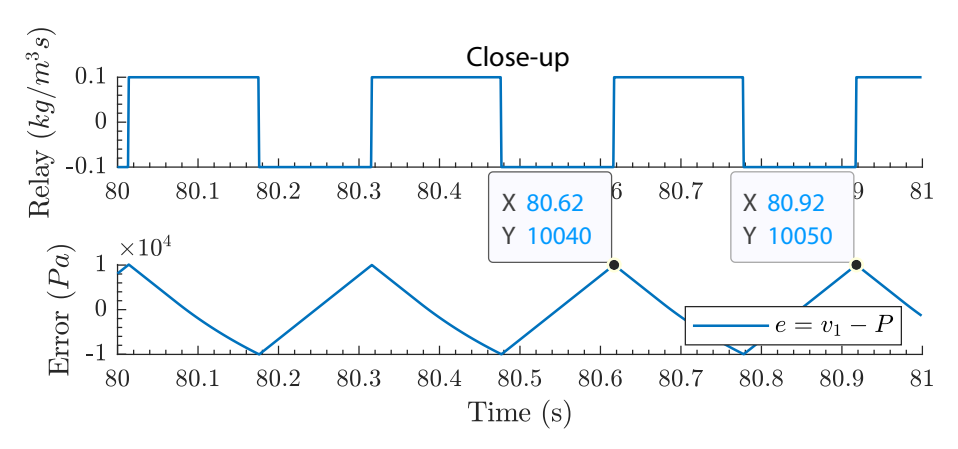


Fig. 5 — Closed up view of the relay input signal and error signal between 80 and 81 s for the PI controller tuning process shown in Fig. 4.

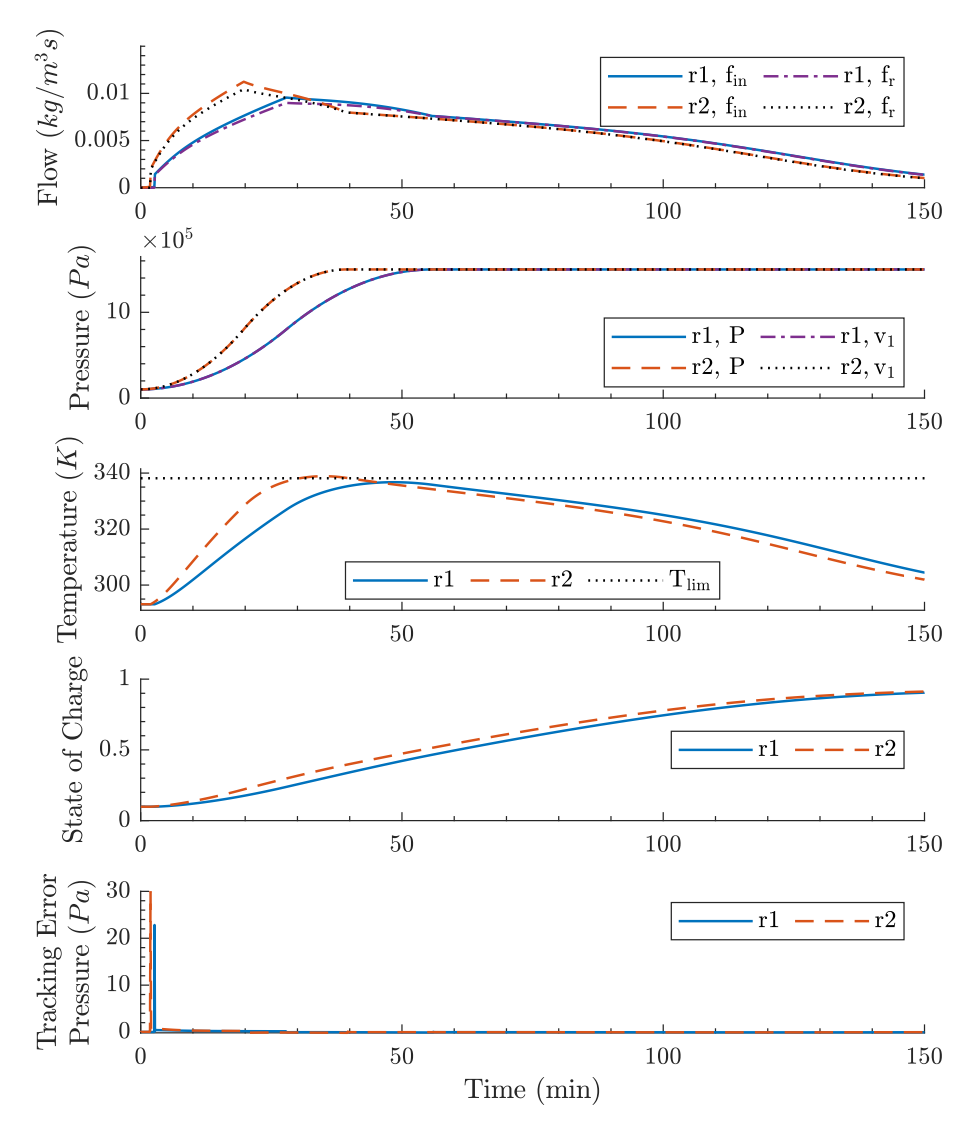


Fig. 6 – Performance of the PI controller for tracking two different transient profile v_1 generated using Eq. (29) with two different r: $r_1 = 0.5$ and $r_2 = 1$.

the PI controller produces larger $f_{\rm in}$ causing the tank pressure to reach the reference pressure quickly. When the SOC is low, from Eq. (5), small pressure difference between P and P_{eq, a}

result in larger absorption reaction, leading T to increase beyond the safety limit $T_{\rm lim}$. When r=0.5, the maximum $f_{\rm in}$ and $f_{\rm r}$ is around 0.01 kg m⁻³ s⁻¹, temperature T is elevated

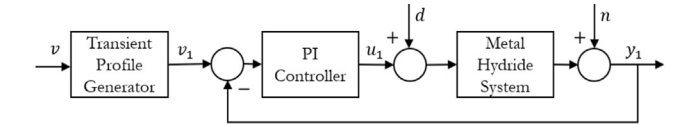


Fig. 7 – Block diagram representation of the MH system with proportional-integral (PI) controller, transient profile generator, load disturbance, and measurement noise.

closed to the temperature limit. Therefore, the mass flow rate $f_{\rm in}$ and the absorption rate $f_{\rm r}$ should be below 0.01 kg m⁻³ s⁻¹ to ensure that the temperature does not exit the temperature limit. The limitation on $f_{\rm r}$ can increase by designing better heat exchanger to dissipate heat quickly.

Performance of PI controller

Fig. 7 illustrates the block diagram of the MH system with a proportional-integral (PI) controller and transient profile generator. In the figure, undesirable inputs are the load disturbance d, which drives the system away from the desired set-point and the measurement noise n, which corrupts the system's information. $u_1 = f_{\rm in}$ is the output of the PI controller, $y_1 = P + n$ is the measured tank pressure with sensing noise, v is the desired set-point, and v_1 is the smooth trajectory generated by the transient profile generator.

The absorption model (Eqs. (21) and (22)) is linearized about the equilibrium point

$$\widetilde{\mathbf{U}} = \begin{bmatrix} \widetilde{\mathbf{u}}_1 \\ \widetilde{\mathbf{u}}_2 \\ \widetilde{\mathbf{u}}_3 \end{bmatrix} = \begin{bmatrix} \mathbf{0} \\ \mathbf{0.1667} \\ \mathbf{293.15} \end{bmatrix}, \ \widetilde{\mathbf{X}} = \begin{bmatrix} \widetilde{\mathbf{x}}_1 \\ \widetilde{\mathbf{x}}_2 \\ \widetilde{\mathbf{x}}_3 \end{bmatrix} = \begin{bmatrix} \mathbf{1.2309} \\ \mathbf{8517.8} \\ \mathbf{293.15} \end{bmatrix}, \tag{55}$$

where \tilde{x}_1 and \tilde{x}_2 are calculated using Eqs. (6)–(8) and

$$\tilde{\mathbf{Y}} = [\tilde{y}_1 \tilde{y}_2]^T = [1.5 \times 10^6 \quad 293.15]^T.$$
 (56)

The linearized model about the equilibrium point, with $\Delta X = X - \widetilde{X}, \, \Delta U = U - \widetilde{U}, \, \text{and} \, \Delta Y = Y - \widetilde{Y}, \, \text{is}$

$$\Delta \dot{\mathbf{X}} = \mathcal{A} \Delta \mathbf{X} + \mathcal{B} \Delta \mathbf{U} \tag{57}$$

$$\Delta \dot{\mathbf{Y}} = \mathcal{C} \Delta \mathbf{X} + \mathcal{D} \Delta \mathbf{U} \tag{58}$$

where

$$\mathcal{A} = \frac{\partial \mathcal{F}}{\partial \mathbf{X} \hat{\mathbf{x}}.\hat{\mathbf{u}}} = \begin{bmatrix} -0.0670 & 0.0165 & 0.0035 \\ 0.1306 & -0.0322 & -0.0068 \\ 0.7066 & -0.1742 & -0.0383 \end{bmatrix}$$
 (59)

$$\mathcal{B} = \frac{\partial \mathcal{F}}{\partial \mathbf{U} \mathbf{x}.\mathbf{u}} = \begin{bmatrix} 1.0262 & 0 & 0\\ 000 - 2.4219 & & \\ & 0 & 0.0016 \end{bmatrix}$$
 (60)

$$C = \frac{\partial \mathcal{G}}{\partial \mathbf{X} \widetilde{\mathbf{X}} \widetilde{\mathbf{U}}} = \begin{bmatrix} 1.2186 & 0 & 0.0051 \\ 0 & 0 & 0 \end{bmatrix} \times 10^6$$
 (61)

$$\mathcal{D} = \frac{\partial \mathcal{G}}{\partial \mathbf{U} \mathbf{x}.\mathbf{u}} = \begin{bmatrix} 0 & 0 & 0 \\ 0 & 0 & 0.8971 \end{bmatrix}$$
 (62)

The transfer function between input $u_1 = f_{in}$ and output $v_2 = P$ is

$$G_{u1,y1} = \frac{1.238 \times 10^6 s^2 + 8.042 \times 10^4 s + 66.16}{s^3 + 0.1376s^2 + 0.0001605s + 4.627 \times 10^{-23}}. \tag{63} \label{eq:Gu1,y1}$$

Recall that the PI controller can be represented in transfer function as

$$G_{c} = K_{p} + K_{i} \frac{1}{c}. {(64)}$$

The transfer functions between n and y_1 and d and y_1 are [41]

$$G_{n, \dot{y}1} = \frac{1}{1 + G_c G_{\dot{y}1, \dot{y}1}}, G_{\dot{d}, \dot{y}1} = \frac{G_{\dot{y}1, \dot{y}1}}{1 + G_c G_{\dot{y}1, \dot{y}1}}.$$
 (65)

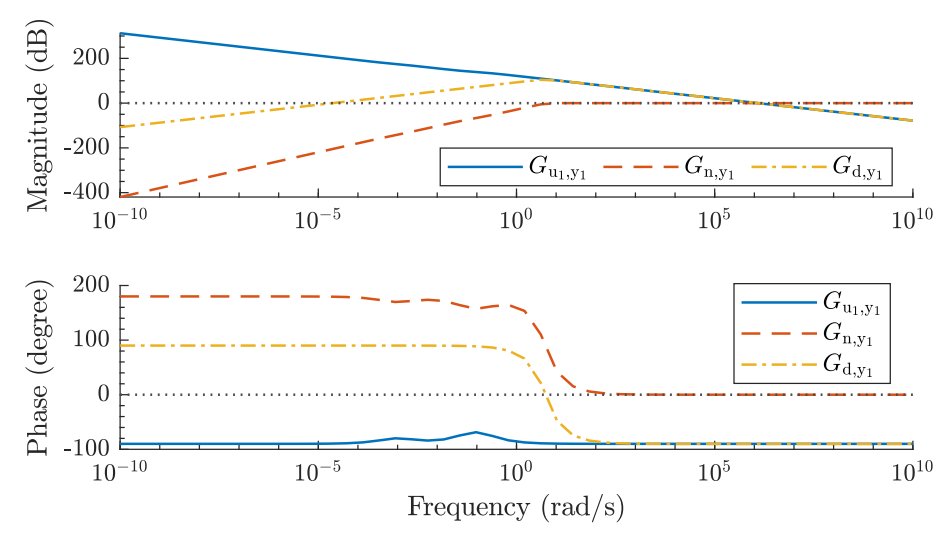


Fig. 8 – Bode diagram representation of the plant transfer function from input u_1 to output y_1 ($G_{u_{-}[1],y_{-}[1]}$), transfer function from measurement noise n to output y_1 ($G_{n,y_{-}1}$), and transfer function from load disturbance d to output y_1 ($G_{d,y_{-}1}$).

The bode diagram for $G_{n,\,y_1}$ and $G_{d,\,y_1}$ along with $G_{u_\{1\},y_\{1\}}$ are presented in Fig. 8. As shown in Fig. 8, with a PI controller, the low frequency measurement noise n below 10 rad s $^{-1}$ are attenuated while higher frequency measurement noise pass through without any changes. In addition, load disturbance d with frequency between 10^{-5} rad s $^{-1}$ to 10^6 rad s $^{-1}$ are amplified up to 104 dB while others are attenuated. Therefore, the PI controller with gain $K_p = 5.7068 \times 10^{-6}$ and $K_i = 2.2827 \times 10^{-5}$ is robust to measurement noise. However, load disturbances with frequency between 10^{-5} rad s $^{-1}$ to 10^6 rad s $^{-1}$ could cause the tank pressure to deviate away from the set-point. Increasing the overall gain of the PI controller will lower the magnitude curve while increasing the cutoff frequency.

Disturbance rejection performance of PI and ADRC controller

From Section Transient profile selection, r = 0.5 generates a good transient profile v_1 for $v = P_{ref}$ which ensures that the pressure P reaches P_{ref} quickly while temperature T remains

within the safety operating limit $T_{\rm lim}$. Also, in Section Transient profile selection, the PI controller demonstrated excellent tracking performance in the absence of load disturbance and measurement noise. Nevertheless, in a practical situation, measurement noise and disturbances due to the error in electrolyzer's mass flow rate and fault of the heat exchanger can occur. A good controller should predict and reject these disturbances while maintaining pressure for charging.

In this section, the performance of the PI controller is examined in the presence of disturbances. For this simulation, the transient profile ν_1 is generated using r=0.5 and $\nu=1.5$ MPa. The PI controller gains are $K_p=5.7068\times 10^{-6}$ and $K_i=2.2827\times 10^{-5}$. The system parameters, initial conditions, and heat exchanger inputs are described in Section on-off control simulation. From Fig. 8, the PI controller is highly influenced by load disturbances between 10^{-5} rad s $^{-1}$ to 10^6 rad s $^{-1}$, therefore, the disturbance added to the inputs $f_{\rm in}$, $f_{\rm w}$, and $T_{\rm w}$, in all have frequency 1 rad s $^{-1}$. The disturbances are.

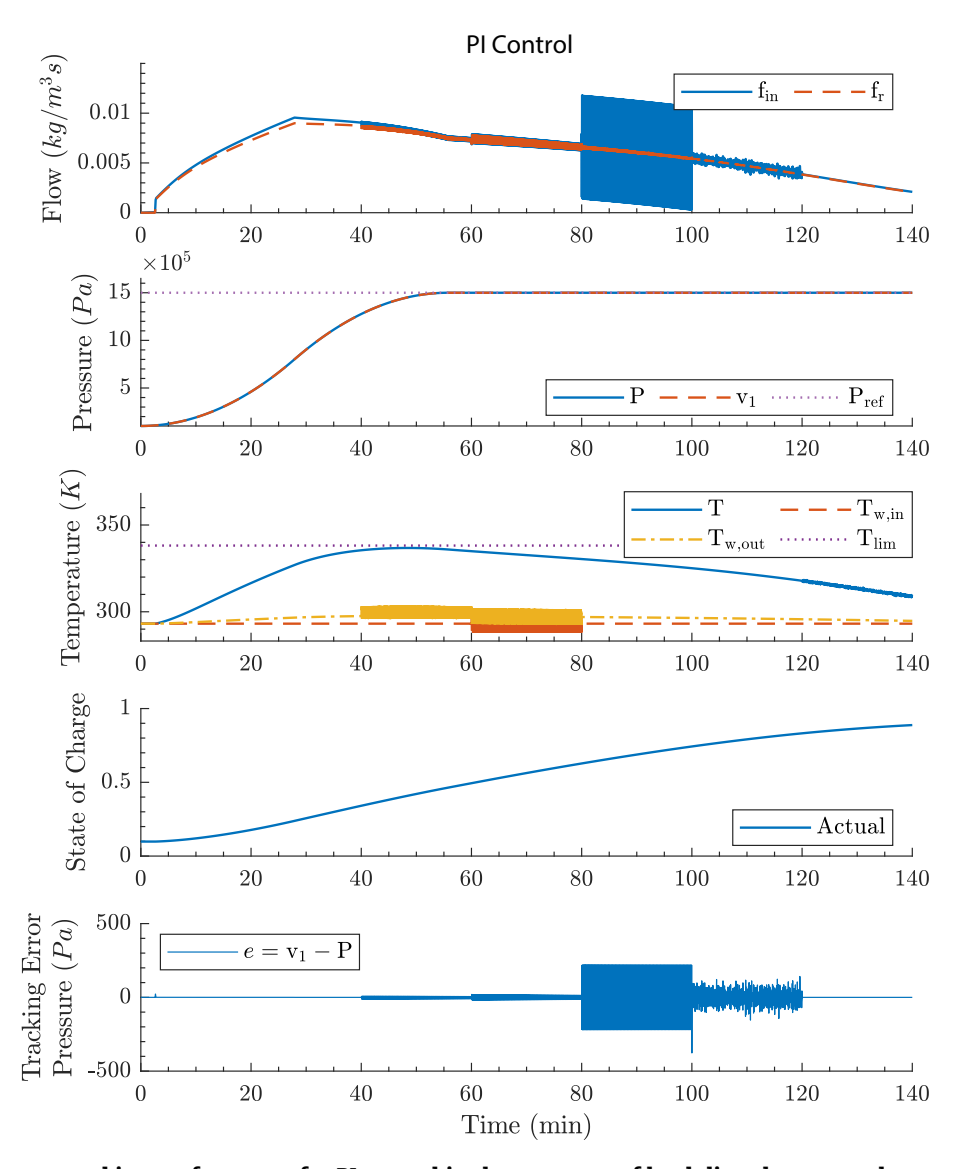


Fig. 9 – The pressure tracking performance for PI control in the presence of load disturbances and measurement noise.

- a) Output P measurement noise: White noise is added to the output P at 100—120 min with power spectral density (PSD) amplitude 1, 000 Pa, correlation time of 1 s, and 23,341 as the starting seed for the random number generator.
- b) Output T measurement noise: White noise is added to the output T at 120—140 min with power spectral density (PSD) amplitude 0.1 K, correlation time of 1 s, and 23,341 as the starting seed for the random number generator.
- c) Unknown coolant flow rate f_w : Disturbance modeled using a sine wave with amplitude 0.1 kg s⁻¹ and frequency of 1 rad s⁻¹ is added to f_w between 20–60 min.
- d) Unknown coolant temperature $T_{\rm w,\;in}$: Disturbance modeled using a sine wave with amplitude 5 K and frequency of 1 rad s⁻¹ is added to $T_{\rm w,\;in}$ between 40–60 min.
- e) Disturbance at tank inlet $f_{\rm in}$: Disturbance modeled using a sine wave with amplitude 0.005 kg m⁻³ s⁻¹ and frequency of 1 rad s⁻¹ is added to $f_{\rm in}$ at 80–100 min.

The performance of the PI controller in rejecting noise is presented in Fig. 9. In the figure, the first graph displays the hydrogen input flow rate f_{in} and absorption reaction rate f_r . The second graph presents the tank pressure P against transient reference v_1 . The third graph shows the tank temperature, the temperature of coolant into and out of the heat exchanger with the temperature limit. The fourth graph gives the SOC of the tank, and the fifth graph provides pressure tracking error. In the simulation results, the mass flow rate f_{in} remains closed to the absorption rate f_r and both are below $0.01 \text{ kg m}^{-3} \text{ s}^{-1}$ when there are no disturbances. The temperature T remains within the temperature limit. As predicted by Fig. 8, the PI controller cannot eliminate load disturbances with frequency 1 rad s^{-1} . The load disturbances added to three inputs $f_{\rm in}$, $f_{\rm w}$, and $T_{\rm w,\ in}$ affect the output P, as shown by the tracking error. The pressure P is not affected by the sensing

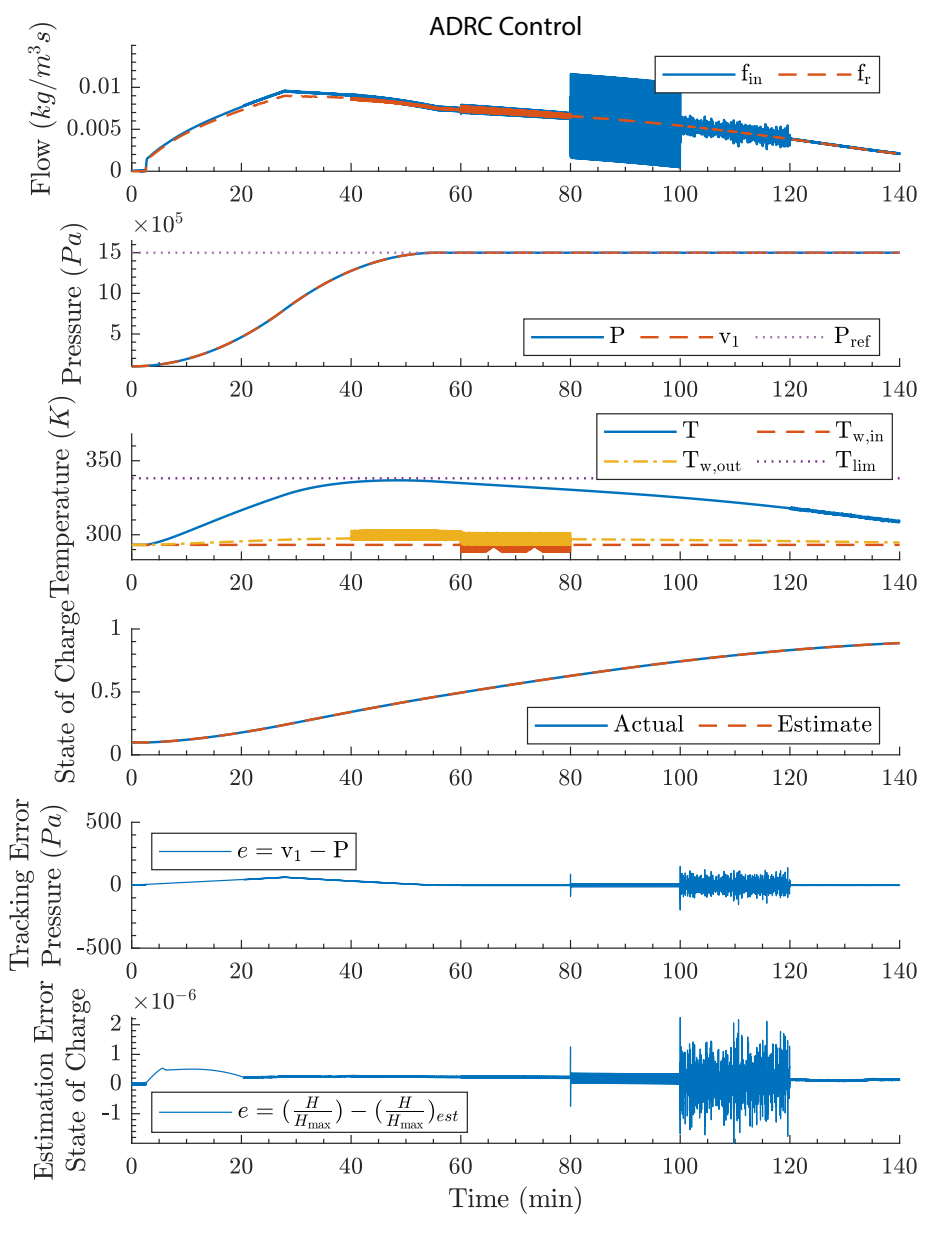


Fig. 10 - The pressure tracking performance for ADRC in the presence of load disturbances and measurement noise.

noise in T as the PI controller does not use temperature data for feedback control.

The simulation is repeated with ADRC using the same conditions described above for comparison. The parameters for the extended state observer are $\beta_{01} = 1$, $\beta_{02} = 1$, 200, $\phi_{01}=$ 0.9, $\phi_{02}=$ 0.7, and the parameters for the nonlinear controller are $\kappa=$ 20, $\psi=$ 0.9. $b=\frac{R}{M_{H_2}}\frac{1}{V_1}T$ as in Eq. (35) The transient profile v_1 is generated using r = 0.5 and v = 1.5 MPa. The performance of the ADRC in rejecting noise is presented in Fig. 10. In the figure, the first graph compares f_{in} against f_r while the second graph shows the pressure in the tank P, the transient profile generated v_1 and the pressure setpoint $P_{ref.}$ The third graph shows the temperature data: the temperature of the tank T, the temperature of the coolant flowing in and out of the heat exchanger, $T_{w, in}$ and $T_{w, out}$, respectively, and the temperature limit T_{lim}. The fourth graph shows the SOC, the fifth graph shows the pressure tracking error, and the sixth shows the SOC estimation error.

The input flow rate $f_{\rm in}$ matches $f_{\rm r}$ to maintain the pressure in the tank at the desired value. Similar to the results of PI controller, the measurement noise added to T does not influence the tracking performance, while measurement noise added to P is not attenuated by the controller. However, unlike the PI controller, ADRC alters the input flow rate $f_{\rm in}$ to eliminate the effect of disturbances added to heat exchanger's input $T_{\rm w,\ in}$ and $f_{\rm w}$ on P. It also reduces the influence of disturbances added to $f_{\rm in}$ resulting in a smooth pressure P. The proposed SOC estimator in Section State-of-charge estimator can predict the SOC of the MH with high accuracy using the extended state observer output z_2 and controller output $f_{\rm in}$ along with measured P and T values. For the estimation error, remains within $e = 2 \times 10^{-6}$.

Both ADRC and PI controllers can track the reference v_1 amidst measurement noise added to P and T. However, the PI controller does not predict and eliminate load disturbances nor estimates SOC. ADRC can predict system SOC and reject undesired load disturbances using an extended state observer and a nonlinear feedback controller. ADRC modifies the input flow rates to cancel the effect of load disturbances added to $T_{\rm w}$, in, $f_{\rm w}$, and $f_{\rm in}$. The simulation result verifies that ADRC's output parameter z_2 and u can estimate SOC accurately as long as parameters for the tank such as V_1 , V_2 , $\rho_{\rm ss}$ and $\rho_{\rm s0}$ are known a priori and measurements for $T_{\rm m}$, $P_{\rm m}$ and $f_{\rm in}$, m are available.

Conclusions

A MH tank can be charged directly by a high-pressure polymer electrolyte membrane (PEM) water electrolyzer. Such configuration saves compression costs and reduces overall system complexity. MH tanks are charged at constant pressure. Therefore, when the water electrolyzer is directly used for charging, the hydrogen production rate should maintain the tank's pressure at the desired pressure for charging. The pressure in the tank is affected by the absorption reaction, which influences tank temperature and MH state-of-charge (SOC).

The active disturbance rejection control (ADRC) contains three parts: reference generator, extended state observer, and nonlinear controller. The reference generator produces a smooth pressure reference profile for the nonlinear controller to track. The generated reference profile prevents abrupt changes in pressure set-point, reduces the spike in absorption reaction, and ensure the tank's temperature is within the safety limit. The extended state observer estimates unknown system disturbance and measurement noise. These estimates are used by the nonlinear controller to produce appropriate control signals to reject the disturbance and noise. The SOC of the MH tank can be accurately determined using system measurements along with estimates given by the extended state observer and controller signal.

Comparisons of the performance between the traditional PI controller and the proposed ADRC controller shows that both controllers can eliminate disturbances originated from the heat exchanger and measurement noise. On the other hand, the ADRC excels in rejecting disturbance produced by the input mass flow rate, maintaining the gaseous pressure in the tank at the desired charging pressure with no oscillations.

Declaration of competing interest

The authors declare that they have no known competing financial interests or personal relationships that could have appeared to influence the work reported in this paper.

Acknowledgment

This research was supported in part by the University of Houston, United States, through a start-up grant and the National Science Foundation, United States, through a REU grant #1659763.

Nomenclature

```
\Delta H
            change in enthalpy (J mol<sup>-1</sup>) for hydrogen absorption
            (-) and desorption (+)
            porosity of the metal alloy
\frac{H}{H_{\text{max}}}
            state-of-charge (SOC) of the metal hydride (MH)
            thermal conductivity (W m^{-1} K^{-1})
            density of gaseous hydrogen in tank (kg m<sup>-3</sup>)

ho_{
m g}
            density of hydrogen (kg m<sup>-3</sup>)

ho_{
m H_2}
            density of unsaturated metal alloy (kg m<sup>-3</sup>)
\rho_{s0}
            density of saturated metal alloy (kg m<sup>-3</sup>)

ho_{	extsf{ss}}
            density of metal hydride (kg m<sup>-3</sup>)
a, b, \Phi, \Phi_0, \beta constants that mathematically represent the
                  metal alloy pressure composition and
                  temperature (PCT) curve
            heat exchange area of the tank (J kg<sup>-1</sup> K<sup>-1</sup>)
A_s
            absorption constant (s^{-1})
C_{a}
C_{\rm d}
            desorption constant (s<sup>-1</sup>)
            specific heat of hydrogen (J kg<sup>-1</sup> K<sup>-1</sup>)
            specific heat of metal hydride (J kg-1 K-1)
C_{p, s}
C_{p, w}
            specific heat of coolant (J kg<sup>-1</sup> K<sup>-1</sup>)
E_{\mathsf{a}}
            activation energy for absorption (J mol<sup>-1</sup>)
E_{\rm d}
            activation energy for desorption (J mol-1)
```

Faraday's constant ($C \text{ mol}^{-1}$)

$f_{ m in}$	flow rate of hydrogen into the tank (kg $\mathrm{m}^{-3}~\mathrm{s}^{-1}$)
$f_{\rm r}$	reaction kinetics (absorption/desorption) of the
	metal alloy (kg $m^{-3} s^{-1}$)
$f_{ m w}$	mass flow rate of the coolant (kg s^{-1})
I	current used for electrolysis (A)
M_{H_2}	molar mass of hydrogen (kg mol ⁻¹)
m_{MH}	mass of the metal alloy (kg)
N_{cell}	number of electrolyzer stack
P	pressure of gaseous hydrogen (Pa)
P_0	reference pressure (Pa)
$P_{\text{eq, a}}$	equilibrium pressure for absorption (Pa)
P _{eq, d}	equilibrium pressure for desorption (Pa)
P_{eq}	equilibrium pressure (Pa)
Q	thermal power exchanges between water and metal
	hydride (W)
R	gas constant (J mol ⁻¹ K ⁻¹)
T	tank temperature (K)
$T_{w, in}$	coolant temperature at the heat exchanger inlet (K)
$T_{w, out}$	coolant temperature at the heat exchanger outlet (K)
U	overall heat transfer coefficient (W K^{-1} m ⁻²)
V_1	normalized volume representing the void space in
	MH tank
V_2	normalized volume of the metal alloy
$V_{H\ 2}$	hydrogen storage capacity of the MH tank (m ³)
V_{MH}	volume of the metal alloy (m ³)
V_{tank}	volume of the tank (m ³)

REFERENCES

- Amos WA. Costs of storing and transporting hydrogen, Tech. rep.. Golden, CO (US): National Renewable Energy Lab.; 1999.
- [2] Durbin D, Malardier-Jugroot C. Review of hydrogen storage techniques for on board vehicle applications. Int J Hydrogen Energy 2013;38(34):14595—617.
- [3] Lototskyy M, Yartys V, Pollet B, Bowman R. Metal hydride hydrogen compressors: a review. Int J Hydrogen Energy 2014;39(11):5818–51.
- [4] Rusman N, Dahari M. A review on the current progress of metal hydrides material for solid-state hydrogen storage applications. Int J Hydrogen Energy 2016;41(28):12108–26. https://doi.org/10.1016/j.ijhydene.2016.05.244.
- [5] Lototskyy MV, Tolj I, Pickering L, Sita C, Barbir F, Yartys V. The use of metal hydrides in fuel cell applications. Prog Nat Sci: Materials International 2017;27(1):3–20. https://doi.org/ 10.1016/j.pnsc.2017.01.008. sI-HYDROGEN STORAGE MATERIALS.
- [6] Rizzi P, Pinatel E, Luetto C, Florian P, Graizzaro A, Gagliano S, Baricco M. Integration of a pem fuel cell with a metal hydride tank for stationary applications. J Alloys Compd 2015;645:S338–42. https://doi.org/10.1016/j.jallcom.2014.12.145. supplement Issue: Proceedings from the 14th International Symposium on Metal-Hydrogen Systems: Fundamentals and Applications, 2014 (MH2014).
- [7] Schlapbach L, Züttel A. Hydrogen-storage materials for mobile applications. Nature (London) 2001;414(6861):353–8.
- [8] Lototskyy MV, Davids MW, Tolj I, Klochko YV, Sekhar BS, Chidziva S, Smith F, Swanepoel D, Pollet BG. Metal hydride systems for hydrogen storage and supply for stationary and automotive low temperature pem fuel cell power modules. Int J Hydrogen Energy 2015;40(35):11491-7.

- [9] Lototskyy MV, Tolj I, Davids MW, Klochko YV, Parsons A, Swanepoel D, Ehlers R, Louw G, [van der Westhuizen] B, Smith F, Pollet BG, Sita C, Linkov V. Metal hydride hydrogen storage and supply systems for electric forklift with lowtemperature proton exchange membrane fuel cell power module. Int J Hydrogen Energy 2016;41(31):13831–42.
- [10] Muthukumar P, Maiya] MP, Murthy SS. Experiments on a metal hydride-based hydrogen storage device. Int J Hydrogen Energy 2005;30(15):1569–81.
- [11] Jensen J, Vestbø A, Li Q, Bjerrum N. The energy efficiency of onboard hydrogen storage. J Alloys Compd 2007;446–447:723–8. https://doi.org/10.1016/ j.jallcom.2007.04.051. proceedings of the International Symposium on Metal-Hydrogen Systems, Fundamentals and Applications (MH2006).
- [12] Marangio F, Pagani M, Santarelli M, Calì M. Concept of a high pressure pem electrolyser prototype. Int J Hydrogen Energy 2011;36(13):7807–15.
- [13] Bolwin K. Application of regenerative fuel cells for space energy storage: a comparison to battery systems. J Power Sources 1992;40(3):307—21.
- [14] Laurencelle F, Dehouche Z, Goyette J, Bose T. Integrated electrolyser—metal hydride compression system. Int J Hydrogen Energy 2006;31(6):762—8.
- [15] Varkaraki E, Lymberopoulos N, Zoulias E, Guichardot D, Poli G. Hydrogen-based uninterruptible power supply. Int J Hydrogen Energy 2007;32(10):1589–96.
- [16] Zhu D, Chabane D, Ait-Amirat Y, N'Diaye A, Djerdir A. Estimation of the state of charge of a hydride hydrogen tank for vehicle applications. In: 2017 IEEE vehicle power and propulsion conference. VPPC); 2017. p. 1–6.
- [17] Pérez-Herranz V, Pérez-Page M, Beneito R. Monitoring and control of a hydrogen production and storage system consisting of water electrolysis and metal hydrides. Int J Hydrogen Energy 2010;35(3):912-9.
- [18] Raju M, Khaitan S. Charging dynamics of metal hydride hydrogen storage bed for small wind hybrid systems. Int J Hydrogen Energy 2011;36(17):10797–807.
- [19] Ogumerem GS, Pistikopoulos EN. Parametric optimization and control toward the design of a smart metal hydride refueling system. AIChE J 2019;65(10):e16680.
- [20] Bhogilla SS, Ito H, Kato A, Nakano A. Experimental study on a laboratory scale totalized hydrogen energy utilization system for solar photovoltaic application. Appl Energy 2016;177:309—22. https://doi.org/10.1016/ j.apenergy.2016.05.145.
- [21] Bhogilla SS, Ito H, Segawa T, Kato A, Nakano A. Experimental study on laboratory scale totalized hydrogen energy utilization system using wind power data. Int J Hydrogen Energy 2017;42(19):13827–38.
- [22] Endo N, Shimoda E, Goshome K, Yamane T, Nozu T, Maeda T. Simulation of design and operation of hydrogen energy utilization system for a zero emission building. Int J Hydrogen Energy 2019;44(14):7118–24. https://doi.org/10.1016/j.ijhydene.2019.01.232.
- [23] Endo N, Shimoda E, Goshome K, Yamane T, Nozu T, Maeda T. Operation of a stationary hydrogen energy system using lifebased alloy tanks under various weather conditions. Int J Hydrogen Energy 2020;45(1):207–15. https://doi.org/10.1016/ j.ijhydene.2019.10.240.
- [24] Cho J-H, Yu S-S, Kim M-Y, Kang S-G, Lee Y-D, Ahn K-Y, Ji H-J. Dynamic modeling and simulation of hydrogen supply capacity from a metal hydride tank. Int J Hydrogen Energy 2013;38(21):8813–28.
- [25] Gonzatti F, Farret F. Mathematical and experimental basis to model energy storage systems composed of electrolyzer, metal hydrides and fuel cells. Energy Convers Manag

- 2017;132:241-50. https://doi.org/10.1016/j.enconman.2016.11.035.
- [26] Zhu D, Ait-Amirat Y, N'Diaye A, Djerdir A. New dynamic modeling of a real embedded metal hydride hydrogen storage system. Int J Hydrogen Energy 2019;44(55):29203–11. https://doi.org/10.1016/j.ijhydene.2019.02.087. special Issue on The 16th International Symposium on Metal-Hydrogen Systems (MH2018), 28 October -2 November 2018, Guangzhou, China.
- [27] MacDonald BD, Rowe AM. Impacts of external heat transfer enhancements on metal hydride storage tanks. Int J Hydrogen Energy 2006;31(12):1721–31.
- [28] Nishizaki T, Miyamoto K, Yoshida K. Coefficients of performance of hydride heat pumps. J Less Common Met 1983;89(2):559–66.
- [29] Åström K, Hägglund T. PID Controllers, Setting the standard for automation. International Society for Measurement and Control; 1995.
- [30] Wang Y-G, Shao H-H. Optimal tuning for pi controller. Automatica 2000;36(1):147–52.
- [31] Han J-Q. Nonlinear design methods for control systems. IFAC Proceedings Volumes 1999;32(2):1531–6.
- [32] Gao Zhiqiang. Active disturbance rejection control: a paradigm shift in feedback control system design. In: 2006 American control conference; 2006. p. 7. https://doi.org/ 10.1109/ACC.2006.1656579.

- [33] Sun D. Comments on active disturbance rejection control. IEEE Trans Ind Electron 2007;54(6):3428-9.
- [34] Hydrogen storage containers on the base of lani 5 -type metal hydrides. URL http://www.labtech-hydrogen.com/.
- [35] Gonzatti F, Miotto M, Farret F. Automation and analysis of the operation of (la0.85ce0.15)ni5 in energy storage plants. Int J Hydrogen Energy 2018;43(5):2850–60. https://doi.org/ 10.1016/j.ijhydene.2017.12.062.
- [36] Gonzatti F, et al. Fundamentos para concepção, controle e automação de uma planta armazenadora de energia utilizando hidrogênio. Ph.D. thesis. Universidade Federal de Santa Maria; 2017.
- [37] Electrolyzer stacks URL https://www.ginerelx.com/electrolyzer-stacks.
- [38] Hang C, Astrom K, Wang Q. Relay feedback auto-tuning of process controllers — a tutorial review. J Process Contr 2002;12(1):143–62.
- [39] äström K, Hägglund T. Revisiting the ziegler—nichols step response method for pid control. J Process Contr 2004;14(6):635–50.
- [40] Ziegler JG, Nichols NB. Optimum settings for automatic controllers. J Dyn Syst Meas Contr 1993;115(2B):220-2.
- [41] Åström KJ. Model uncertainty and robust control. Lecture Notes on Iterative Identification and Control Design; 2000. p. 63-100.